RSC Advances

A comparative *ab initio* study to investigate the rich structural variety and electronic properties of Ga_mTe_n (m = 1,2 and n = 1–4) with analogous oxides, sulfides and selenides.

N. Seeburrun[a], I. A. Alswaidan[b], H.-K. Fun[b,c], E. F. Archibong[d], P. Ramasami[a,*]

[a] *Computational Chemistry Group, Department of Chemistry, Faculty of Science, University of Mauritius, Réduit, Mauritius*

[b] *Department of Pharmaceutical Chemistry, College of Pharmacy, King Saud University, P.O. Box 2457, Riyadh 11451, Saudi Arabia*

[c] *X-ray Crystallography Unit, School of Physics, Universiti Sains Malaysia, 11800 USM, Penang, Malaysia*

[d] *Department of Chemistry and Biochemistry, University of Namibia, Namibia*

[*] Author for correspondence e-mail; p.ramasami@uom.ac.mu

Fax: +230 4656928

Tel: +230 4657507

Abstract

A series of gallium telluride, Ga_mTe_n (m = 1,2 and n = 1–4), clusters has been examined by using density functional theory (DFT), second-order Møller−Plesset perturbation theory (MP2) and the coupled cluster approach with single and double substitutions and a perturbative treatment of triple excitations [CCSD(T)]. The study unravels the question of whether neutral $GaTe_2$ is isostructural with BO_2 as earlier proposed by experiment (Trans. Faraday Soc. **1968**, *64*, 2998). The results of gallium tellurides are compared with the oxygen, sulfur and selenium analogies. In most cases, the substitution of O/S/Se by Te atoms in the gallium clusters does not affect drastically the structural characteristics. The adiabatic electron affinities (AEAs) of Ga_mTe_n (m = 1,2 and n = 1–4) clusters range from 1.33 to 3.46 eV at the CCSD(T)//B3LYP level. The AEAs of gallium tellurides are found to be independent on the electrophilicity of the clusters. Further, the adiabatic ionization potentials (AIPs) of the clusters are in good agreement with available experimental data. This research is expected to provide insight into the structural characteristics and electronic properties of gallium chalcogenides.

Keywords: *Gallium tellurides, electronic structures, adiabatic electron affinities, adiabatic ionization potentials*

1. Introduction

Gallium chalcogenides have attracted scientific and commercial interest because they are semiconducting materials with extensive technological applications. The interaction between gallium and tellurium atoms is of prime importance due to their wide usage in optoelectronic and photovoltaic devices [1,2]. Gallium monotelluride, GaTe is a heteronuclear gallium telluride which has been mostly studied [3]. Owing to its band gap of around 1.7 eV, GaTe is useful in photoelectronic devices, radiation detectors [1,2], field-effect transistors and phototransistors [4]. Doped gallium telluride clusters such as $AgGaTe_2$ is used in thin film solar cells [5], $CuGaTe_2$ as a high-performance thermoelectric material [6] and $LiGaTe_2$ for optical applications [7]. Neutral telluroether complexes containing gallium atoms are used in chemical vapor deposition [8,9] and as phase change memory materials [10].

Extensive efforts have been devoted in the study of gallium chalcogenide clusters [1–24]. Experiment and high level computations have shown GaO_2 to be linear [22,23]. However, theoretical results reveal that GaS_2 and $GaSe_2$ adopt cyclic geometries while anionic GaX_2 (X = O–Se) prefers a linear configuration ($D_{\infty h}$) [11–15]. The lowest energy structure of neutral and anionic GaX_4 (X = O–Se) possess a kite-shape with a trichalcogenide unit [14–16]. Ga_2Se and Ga_2Te adopt bent configurations [11,16] unlike Ga_2O which is linear [12]. For neutral and anionic Ga_2X_3 (X = O–Te) [13,17,19,20], a V-shape and kite-shape are obtained, respectively. In the case of the Ga_2X_3 (X = O–Te) [13,17,19,20] series, a decrease in the adiabatic electron affinity (AEA) values is noted at the CCSD(T)//B3LYP level of theory. Ga_2X_4 and their respective anions (X = O–Se) have similar ground-state geometries [15,16,21]. Structural differences are observed when Ga_3X_2 (X = O−Te) clusters are compared. Neutral Ga_3O_2 [17] and Ga_3S_2 [15] adopt kite-shape geometries while Ga_3Se_2 and Ga_3Te_2 adopt three-dimensional structures with D_{2h} and C_{2v} symmetries [20,22]. In the same vein, $Ga_3S_2^-$, $Ga_3Se_2^-$ and $Ga_3Te_2^-$ [16,19,24] prefer three-dimensional structures with a D_{3h} symmetry differing from the planar kite geometry of $Ga_3O_2^-$ [17].

In view of the above, structural and electronic changes are highlighted by substitution of atoms. Fueled by these interesting results and an urge to see whether significant differences are noted on going down the periodic table, a systematic theoretical investigation of gallium tellurides, Ga_mTe_n (m = 1,2 and n = 1–4) was embarked to assess the structural and electronic properties. The objectives of the research are: (i) to study the equilibrium structures; (ii) to provide a reliable theoretical prediction of the relative stabilities, harmonic vibrational frequencies and energetic features such as electron detachment energies, electron affinities and ionization potentials (iii) to compare the ground state geometries and variations in the electronic properties with analogues oxides, sulfides and selenides and (iv) to compare the electron affinities of gallium telluride clusters with chlorine atom in order to determine whether they can be classified as superhalogens.

2. Computational methods

The computations of mono and digallium telluride, Ga_mTe_n (m = 1,2 and n = 1–4), clusters were performed with the Gaussian 09 [25] program. To obtain the ground state structures, various initial geometries were taken from isoelectronic gallium oxides, sulfides and selenides

[14−21] [Figs. 1−5]. Based on previous investigations [12,14,15−17,19−21], the 6-311+G(2df) one-particle basis set was employed for Ga atom while the LANL2DZdp ECP [26] and def2-TZVP triple split valence basis sets [27] were used for Te atom. The density functional theory (DFT) with the B3P86, B3PW91 and B3LYP functionals [28−33] and the MP2 [34,35] level of theory were employed. The single point CCSD(T) [36] computations were performed using optimized geometries from the B3LYP functional.

The adiabatic electron affinity (AEA), adiabatic detachment energy (ADE), vertical detachment energy (VDE), adiabatic ionization potential (AIP), vertical ionization potential (VIP) and chemical hardness (η) were calculated as follows:

AEA = E (optimized neutral at ground state) − E (optimized anion at ground state);

ADE = E (optimized corresponding neutral) − E (optimized anion);

VDE = E (neutral at optimized anion geometry) − E (optimized anion);

AIP = E (optimized cation at ground state) − E (optimized neutral at ground state);

VIP = E (cation at optimized neutral geometry) − E (optimized cation);

$\eta \approx (\mathrm{VIP} - \mathrm{VDE})/2$

The harmonic vibrational frequencies of the optimized geometries were analyzed to ensure that all the ground state structures belong to the minima on the potential energy surface. The Natural Bond orbital (NBO) analysis [37,38] was performed with the B3LYP functional to provide insight into the nature of bonding in the clusters. The HOMO-LUMO gaps and chemical hardness (η) of the neutral gallium tellurides were also calculated with the B3LYP functional. In addition, the dissociation energies (D_e) of the studied clusters were carried out.

3. Results and discussion

Optimized geometrical configurations of the lowest energy states of gallium telluride clusters, Ga_mTe_n (m =1,2 and n = 1–4) are shown from Figs. 1–5. The energetic data (ΔE) is listed in Table 1. The internal coordinates and harmonic vibrational frequencies of the ground state geometries are available in Tables S1–S8 (Supporting Information). The AEA and AIP values are presented in Tables 2 and 3. The dissociation energies (D_e) of the gallium tellurides are shown in Table 4. The Natural Bond orbital (NBO) [34,35] on the gallium atoms are summarized in Table S9 while the VDE and chemical hardness (η) are given in Table S10.

A. Structural properties.

The electronic ground state of neutral GaTe is $^2\Sigma^+$, which is in agreement with GaO [38] and GaSe [16]. The quartet and sextet states of GaTe are well separated from the doublet ground state by 2.68 and 5.23 eV, respectively at the CCSD(T)//B3LYP level. The most stable electronic states of $GaTe^-$ and $GaTe^+$ are $^1\Sigma^+$ and $^3\Sigma^+$ (Fig. 1), respectively. This result is consistent with anionic and cationic GaO [39] and GaSe [16]. A cyclic structure is found as the lowest energy structure for $GaTe_2$ with the DFT and MP2 methods. However, single point CCSD(T) using DFT and MP2 geometries, reveals a linear structure (Fig. 2) by analogy with BO_2 [11]. This ambiguity was solved with def2-TZVP [27], being a large basis set. Single point CCSD(T) computations with def2-TZVP basis set reveals a cyclic structure for $GaTe_2$. Furthermore, the linear structure is a saddle point with the MP2 method. In this vein, the linear structure of $GaTe_2$ is the first low-lying isomer. For the tri-atomic series, $GaTe_2$ is cyclic as GaS_2 [15] and $GaSe_2$ [16] while GaO_2 is linear [22,23].

Akin to GaO_2^- [12], GaS_2^- [15] and $GaSe_2^-$ [16], anionic $GaTe_2$ prefers a linear centrosymmetric ($D_{\infty h}$) configuration. The first low-lying geometry of $GaTe_2^-$ is bent ($^1A_1$). As its selenide congener [16], cationic $GaTe_2$ adopts a bent configuration with a C_s symmetry. The lowest-energy configuration of neutral, negatively and positively charged $GaTe_3$ consists of a diatomic GaTe molecule bound perpendicularly to a Te_2 moiety (Fig. 3). Similar neutral and anion ground state geometries were reported for gallium selenide clusters [16]. Neutral, negatively and positively charged $GaTe_3$ adopt a rhombic structure as the first low lying isomer. $GaTe_4$ and its anion adopt kite geometries with a tritelluride unit ($^2B_1$) analogous to gallium oxide [14], sulfide [15] and selenide [16]. This result is further confirmed by the CCSD(T)//B3LYP and CCSD(T)//MP2 computations. The low-lying structure of neutral and anionic $GaTe_4$ is of D_{2d} symmetry, which is the lowest-energy structure for $GaTe_4^+$. On the other hand, the low lying structure of $GaTe_4^+$ adopts the kite geometry which is 0.63 eV above the ground state geometry with the MP2 level.

The lowest-energy state of neutral Ga_2Te is $^2A_2$ with a bent configuration (C_{2v}) (Fig. 2). This result is consistent with Uy *et al*. [11]. This geometry is isostructural with Ga_2Se [16] but differs from Ga_2O, which is linear [12]. The next low-lying geometry of Ga_2Te is linear. Anionic and cationic Ga_2Te maintain the bent configuration of the neutral species but with C_{2v} and C_s symmetries, respectively. Same behavior was pointed out with gallium selenide [16]. A distinct difference is noticed within the Ga_2X_2 (X = O–Te) family as Ga_2O_2 is linear [12], Ga_2S_2 is rhombic [15], Ga_2Se_2 is L-shape [16] and Ga_2Te_2 has a butterfly structure with a C_{2v} symmetry (Fig. 4). The structure of $Ga_2Te_2^-$ is rhombic, which is analogous to $Ga_2O_2^-$ [12], $Ga_2S_2^-$ [15] and $Ga_2Se_2^-$ [16]. For $Ga_2Te_2^+$, a L-shape structure is obtained as $Ga_2Se_2^+$ [16]. The low lying isomers for neutral, anionic and cationic Ga_2Te_2 adopt linear, cyclic and L-shape configuration, respectively. The lowest-energy structure of neutral and anionic Ga_2Te_4 can be viewed as rhombic with terminal one tellurium atom attached to each gallium atom (D_{2h}) (Fig. 5). Similar ground state geometry was found with gallium oxide [21], sulfide [15] and selenide [16]. $Ga_2Te_4^+$ adopts a similar 'fish-like' structure as $Ga_2Se_4^+$ [16]. The next energetically low-lying isomer of Ga_2Te_4 is a 'fish-like' structure which is 0.44 eV above the ground state geometry (MP2). The low lying isomer of anionic Ga_2Te_4 is a twisted hexagon configuration and cationic Ga_2Te_4 prefers a planar configuration with D_{2h} symmetry. Gallium telluride clusters prefer planar structures with the exception of mono and digallium tetratelluride cations. A structural evolution is revealed upon addition of a tellurium atom to the $GaTe_n$ and Ga_2Te_n series (Figs. S1 and S2). The NBO charges on gallium atoms are positive with the exception of $GaTe^-$ and $Ga_2Te_4^+$ (Table S9). No significant pattern is observed in the natural charge of gallium atom upon sequential addition of tellurium atoms with the exception of $GaTe_n^+$ and $Ga_2Te_n^-$.

B. Geometrical properties.

Akin to GaO [38] and GaSe [16], a slight elongation of 0.072 Å (B3LYP) and 0.095 Å (MP2) is observed in the monotelluride Ga−Te bond length from GaTe to $GaTe^-$. As expected, an increase in the bond angle at the apex is observed with the cyclic structure of GaO_2 (38.0°) [12], GaS_2 (47.5°) [15], $GaSe_2$ (51.0°) [16] and $GaTe_2$ (55.4°) [B3LYP]. Unlike the GaX_3/GaX_3^- (X = O and Se) [16,18] system, addition of an electron to $GaTe_3$ shortens the terminal Ga–Te bond length (DFT and MP2). On the other hand, there is an increase in the terminal Ga–Te bond from $GaTe_3$ to $GaTe_3^+$. Like gallium selenide [16], the bridge Ga–Te bond is elongated whereas the terminal Ga–Te bond is shortened from $GaTe_4$ to $GaTe_4^-$ (DFT and MP2). However, the reverse pattern was observed with the gallium oxide [14] and sulfide [15] congener. For the GaX_4 (X = O–Te) [14–16] series, a compression in the bond angle of the trichalcogenide unit is noted in all cases. Turning to the Ga_2Te_n series, the Ga–Te–Ga bond angle compresses (DFT and MP2) from Ga_2Te to Ga_2Te^-. Similar finding was found with gallium oxide [12] and selenide [16]. Upon addition of an electron to Ga_2Te_2, the three-dimensional structure turns into a planar configuration unlike Ga_2Se_2 [16] where both neutral and cation maintain the planar L-shaped geometry. The bridge Ga–Te bonds of Ga_2Te_4 are slightly shorter than the anion whereas the terminal Ga–Te bonds are longer. The bond angle between the terminal Ga–Te and neighboring tellurium atom of Ga_2Te_4 is smaller than that of Ga_2O_4 [21], Ga_2S_4 [15] and Ga_2Se_4 [16].

The Ga–Te bond lengths of the neutral gallium tellurides are within the range 2.357–2.845 Å (B3P86), 2.331–2.851 Å (B3PW91), 2.342–2.884 Å (B3LYP) and 2.316–2.791 Å (MP2). The Ga–Te bond lengths of the gallium tellurides are in agreement with mixed chalcogenide cubanes [40], KGa_2Te_6 [41], monoclinic GaTe [42,43], hexagonal GaTe [44], Ga_2Te_5 [45] and telluroether gallium complexes [9]. The Te–Te bond lengths of the neutral gallium tellurides are within the range 2.662–2.776 Å (B3P86), 2.663–2.777 Å (B3PW91), 2.680–2.827 Å (B3LYP) and 2.681–2.905 Å (MP2). The Te–Te bond lengths of the gallium tellurides are smaller than that of contact ion pair of tellurium system [45].

C. Vibrational properties.

All the ground state geometries of the gallium telluride clusters have real frequencies. The frequencies of GaTe with DFT functionals (257 cm^{-1} and 242 cm^{-1}) agree very well with Uy *et* *al*. (250 cm^{-1}) [11]. Like GaSe [16], the stretching frequency of GaTe and $GaTe^{-}$ are close to each other. From Uy *et al*. [11] investigation, $GaTe_2$ has three vibrational frequencies 152, 104 and 92 cm^{-1}, respectively. With linear $GaTe_2$, four wavenumbers were achieved and this feature negates its possibility as ground-state geometry. The theoretical vibrational frequencies are higher than the experimental values with the DFT and MP2 methods. The highest frequency mode of $GaTe_3$ is attributed to the symmetrical stretching of terminal Ga–Te bond. Same observations were noted for GaO_3 [18] and $GaSe_3$ [16]. The highest frequency mode of GaX_4 (X = O−Te) [12,14−16] corresponds to the stretching of X−X bond. Turning to digallium chalcogenides, the most active mode of Ga_2X (X = O, Se, Te) [12,16] is the asymmetrical stretching of Ga–X bond. However, the harmonic vibrational frequencies of Ga_2Te are not in good correlation with the values reported by Uy *et al.* [11]. Smaller wavenumbers are obtained with the DFT and MP2 levels of theory (Table S2, S4, S6 and S8). The highest frequency vibrations of Ga_2X_2 and Ga_2X_4 (X = O−Te) [12,15,16,21] correspond to the stretching of X−X and terminal Ga–X bond, respectively. No significant pattern is observed in the frequencies upon sequential addition of tellurium atom to the $GaTe_n$ and Ga_2Te_n (n = 1−4) series.

D. Electronic properties.

I. Adiabatic electron affinities (AEAs)

The AEA of GaTe ranges from 2.46 eV [CCSD(T)//B3LYP] to 3.20 (B3P86). The AEA of GaTe at the CCSD(T) level is same as reported with the single point CCSD(T)//B3LYP with LANL2DZdp basis set. The ground state electronic configuration of $GaTe_2^{-}$ is $(6\sigma_g)^2(6\pi_u)^2(4\pi_g)^2(4\sigma_u)^2(2\delta_g)^2$. The AEA of $GaTe_2$ varies from 3.23 eV (B3LYP) to 3.83 eV

(B3P86). The excess electron of $GaTe_2^-$ is distributed over the tellurium atoms (Fig. S3). Similar HOMO plots were observed for GaX_2^- (X = S and Se) [15,16]. The electronic configuration of $GaTe_3^-$ is $(12a_1)^2(6b_2)^2(5b_1)^2(2a_2)^2$ and that of $GaTe_4^-$ is $(13a_1)^2(7b_2)^2(6b_1)^2(2a_2)^2$. Their AEA values range from 3.20 to 3.94 and 3.10 to 3.81 eV, respectively. Akin to gallium selenide [16], the excess electron of $GaTe_3^-$ and $GaTe_4^-$ is localized on the terminal tellurium atom (Fig. S3).

The electronic configuration of Ga_2Te^- is $(14a_1)^1(12b_2)^2(5b_1)^2(4a_2)^2$ and the electron detachment process of $^1A_1$ (C_{2v}) + e^- ← $^2A_1$ (C_{2v}) involves the removal of an electron from the $14a_1$ molecular orbital (MO) to yield the $^1A_1$ (C_{2v}) ground state of Ga_2Te. The AEAs of Ga_2Te vary from 1.25 eV (B3LYP) to 1.92 eV (B3P86). The lowest-lying doublet state of $Ga_2Te_2^-$ has an electronic configuration of $(10a_g)^2(9b_{2u})^1(5b_{1u})^2(4b_{3u})^2(4b_{3g})^2(3b_{1g})^2(2b_{2g})^2(1a_u)^2$ and the AEAs vary from 2.34 [CCSD(T)//B3LYP] to 2.95 eV (B3P86). Like the sulfur [15] and selenium [16] analogies, the extra electron of $Ga_2Te_2^-$ is distributed over the bridge tellurium atoms (Fig. S4). The electronic configuration of anionic Ga_2Te_4 is $(11a_g)^2(10b_{1u})^2(6b_{2u})^2(5b_{3g})^1(4b_{2g})^2(2b_{3u})^2(2b_{1g})^2(1a_u)^2$ and transition $^3B_{1u}$ (D_{2h}) + e^- ← $^2B_{2g}$ (D_{2h}) involves the removal of a b_{2u} electron from the anion to produce the $^3B_{1u}$ (D_{2h}) ground state of Ga_2Te_4. The AEAs range from 3.01 eV to 4.07 eV. For the Ga_2X_4 (X = O–Te) [15,16,21] series, the extra electron of the anion is localized around the terminal chalcogen atoms (Fig. S4). The ADEs and AEAs are the same for the studied gallium telluride clusters, with the exception of Ga_2Te_2 and Ga_2Te_3, because of the similar ground state geometry of the neutral and anion.

A significant increase in the AEA values is seen when progressing from Ga_2Te to Ga_2Te_4 (Fig. 6). This trend was observed with gallium oxides [21], sulfides [15] and selenides [16].

Similar increase in the AEAs is expected for the $GaTe_n$ series but instead, a drop in the electron affinity values is obtained for $GaTe_3$ and $GaTe_4$ (Fig. 6). Among the gallium tellurides, $GaTe_2$ has the highest electron affinity at the CCSD(T)//B3LYP level of theory. However, the electron affinity of $GaTe_2$ is less than chlorine atom (3.62 eV) [46] with different levels of theory and it has a VDE of 3.42 eV with the B3LYP functional. This is obvious due to electronegativity values. In this vein, unlike analogous gallium oxide [12], sulfide [15] and selenide [16], $GaTe_2$ cannot exhibit superhalogen properties. The AEA of the Ga_2X_2 (X = O−Te) system is the lowest among the series studied (Fig. S5). No significant trend is observed in the AEA values, with of exception Ga_2X_3, when changing the O/S/Se substituents to Te [12−17,19−22]. This clearly demonstrates that the electron affinity of gallium chalcogenide clusters is independent of electronegative atoms in the system but is related to the electronic structures.

II. Adiabatic ionization potentials (AIPs)

The calculated AIPs of GaTe and $GaTe_2$ are in accordance with the experimental data [11]. In the case of GaTe, the B3PW91 functional provides a reliable theoretical value while for $GaTe_2$, the B3P86 yields a value closer to the experimental one. The AIP values of $GaTe_3$ range from 6.85 [CCSD(T)//B3LYP] to 7.84 (B3P86) eV and $GaTe_4$ from 6.45 (MP2) to 7.64 (B3P86) eV. Turning to digallium telluride series, the AIP of Ga_2Te ranges from 7.54 (MP2) to 8.21 eV (B3P86), Ga_2Te_2 from 7.13 (CCSD(T)//B3LYP) to 8.22 (B3P86) eV, Ga_2Te_3 from 6.86 [CCSD(T)/B3LYP] to 7.66 (B3P86) eV and Ga_2Te_4 from 6.80 (MP2) to 7.54 (B3P86) eV. As expected, the AIP results of Ga_2Te and Ga_2Te_2 are consistent with Uy *et al*. [11] experimental data. The AIPs of the gallium tellurides are lower than the gallium selenides [16]. As shown in Fig. 7, the AIPs decrease upon sequential addition of tellurium atom to the $GaTe_n$ series. This shows that AIP is not only related to the total number of tellurium atoms but also on electronic structures. Similar observation was highlighted with AEA.

III. Mean unsigned error (MUE)

The accuracies of the different methods used in the research were examined by calculating the mean unsigned error (MUE) [47]. The single point CCSD(T)//B3LYP values with the def2-TZVP basis set were taken as reference data. With the AEA values, the MUE was 0.56 eV (B3P86), 0.07 eV (B3PW91), 0.10 eV (B3LYP), 0.18 eV (MP2) and 0.19 eV CCSD(T)//B3LYP with the LANL2DZdp basis set. Similarly, the MUE of the studied gallium tellurides was calculated by using the AIPs values. The calculated MUE is 0.85 eV (B3P86), 0.07 eV (B3PW91), 0.13 eV (B3LYP), 0.17 eV (MP2) and 0.23 eV CCSD(T)//B3LYP with the LANL2DZdp basis set. In both cases, the B3PW91 functional gives meaningful values.

IV. HOMO–LUMO gaps

The HOMO–LUMO gaps of neutral gallium telluride clusters are shown in Table S10. A large value of the HOMO–LUMO energy gap enhances chemical stability of the cluster [48]. The HOMO–LUMO gaps for the lowest-energy configurations are large, varying from 2.61 ($GaTe_4$) to 3.99 eV (GaTe) with the B3LYP functional. For the $GaTe_n$ series, a general decrease in the HOMO–LUMO gaps is noted with an increase in the tellurium-to-metal ratio. However, no correlation is observed for the Ga_2Te_n series. Even though the substitution of O/S/Se by Te does not lead to a significant trend for the HOMO–LUMO energy gap, a decrease in the HOMO–LUMO energy gap values is noted for the Ga_2X_3 and Ga_2X_4 [15,16,18,21] series.

V. Chemical hardness (η)

Pearson states: 'Clusters arrange their electronic structures so as to have the maximum possible hardness' [49]. The chemical hardness of the gallium tellurides varies from 1.58 to 3.19 eV with the B3LYP functional (Table S10). An increase in the tellurium-to-metal ratio decreases the chemical hardness of the Ga_2Te_n clusters. The HOMO−LUMO gaps can be related to hardness (η). Clusters with small HOMO−LUMO gaps are said to be 'soft' [50]. As mentioned earlier, the HOMO−LUMO gaps of some studied gallium tellurides are relatively large and thereby they can be considered as 'hard' clusters.

E. Thermodynamic Stability.

The dissociation energy (D_e) is obtained as the difference in total energies of the initial state and the sum of total energies of the decay fragments. The dissociation energies are positive indicating that the clusters are stable (Table 4). The D_e values of GaTe are in agreement with the experimental data (222–272 kJ/mol) [11]. To compare the chalcogen effect for GaX (X = O−Te) series, the D_e of GaO and GaS were calculated. The D_e of GaX [16] decreases with increasing atomic number of the chalcogen element. This implies that it is easier to cleave a Ga−Te than a Ga−O bond. The monogallium tellurides, with the exception of GaTe, favour a cascade release of tellurium molecule. The dissociation of Ga_2Te_4 results into Ga_2Te_2 and a Te molecule. This is because the terminal tellurium atoms are cleaved easier compared to bridge tellurium ones. Similar feature was observed for gallium sulfide and selenide [15,16,21]. The D_e of the preferred channel decreases upon sequential addition of tellurium atom to $GaTe_n$ and Ga_2Te_n series. Similar observation was seen with selenium analogues [16].

4. Conclusions

Using a number of computational methods, the structural and electronic properties of gallium telluride Ga_mTe_n (m = 1,2 and n = 1–4) clusters were investigated. One prime focus was to explore the substitution of O/S/Se by Te in the gallium clusters. The substitution of O/S/Se by Te in the studied gallium tellurides does not induce much structural changes. A structural divide is observed for the Ga_2X_2 (X = O−Te) series where Ga_2O_2 is linear, Ga_2S_2 is rhombic, Ga_2Se_2 is L-shape and Ga_2Te_2 has a butterfly structure. The reported Ga–Te bond lengths, AIPs and D_e are found to be in agreement with experimental data. The B3PW91 functional was found to provide more reliable data as it gives a smaller mean unsigned error. This is further confirmed from AIP values. Akin to gallium selenide clusters, the AEAs and AIPs of gallium tellurides are not solely related to the total number of tellurium atoms but also dependant on electronic structures. In contrast to analogous GaO_2, GaS_2 and $GaSe_2$, $GaTe_2$ is not classified as a superhalogen because it has lower AEA and VDE values than chlorine atom. The results of this research show that the substitution of an atom by another can open the door to novel structural and electronic properties.

5. References

1. O. Madelung, R. Poerschke, *Semiconductors: Other than Group IV Elements and III-V Compounds*; Springer-Verlag: Berlin, 1992.
2. M. A. Malik, M. Afzaal, P. O' Brien, *Chem. Rev.*, 2010, ***110***, 4417.
3. A. Zubiaga, F. Plazaola, J. A. García, C. Martínez-Tomás, V. Muñoz-Sanjosé, *Phys. Rev. B*, 2010, ***81***, 195211.

4. Z. Wang, K. Xu, Y. Li, X. Zhan, M. Safdar, Q. Wang, F. Wang, J. He, *ACS Nano*., 2014, ***8***, 4859.
5. K. Aravinth, A. G. Babu, P. Ramasamy, *Mater. Sci. Semicond. Process*, 2014, ***24***, 44.
6. K. Kurosaki, S. Yamanaka, *Phys. Status Solidi A*, 2013, ***210***, 82.
7. L. Isaenko, P. Krinitsin, V. Vedenyapin, A. Yelisseyey, A. Merkulov, J. -J. Zondy, V. Petrov, *Cryst. Growth Des*., 2005, ***5***, 1325.
8. K. George, C. H. K. De Groot, C. Gurnani, A. L. Hector, R. Huang, M. Jura, W. Levason, G. Reid, *Phys. Procedia*, 2013, ***46***, 142.
9. K. George, C. H. K. De Groot, C. Gurnani, A. L. Hector, R. Huang, M. Jura, W. Levason, G. Reid, *Chem. Mater.,* 2013, ***25***, 1829.
10. H. Zhu, J. Yin, Y. Xia, Z. Liu, *Appl. Phys. Lett*., 2010, ***97***, 083504.
11. O. M. Uy, D. W. Muenow, P. J. Ficalora, J. L. Margrave, *Trans. Faraday Soc*., 1968, ***64***, 2998.
12. S. Gowtham, A. Costales, R. Pandey, *J. Phys. Chem. B*, 2004, ***108***, 17295.
13. J. J. BelBruno, E. Sanville, A. Burnin, A. K. Muhangi, A. Malyutin, *Chem. Phys. Lett*., 2009, ***478***, 132.
14. E. F. Archibong and P. Ramasami, *Comp. Theo. Chem.*, 2011, ***964***, 324.
15. N. Seeburrun, H. H. Abdallah, E. F. Archibong, P. Ramasami, *Struc. Chem.*, 2014, ***25***, 755.
16. N. Seeburrun, E. F. Archibong, P. Ramasami, *J. Mol. Model*., 2015, ***21***, 42.
17. E. F. Archibong, E. N. Mvula, *Chem. Phys. Lett*., 2005, ***408***, 371.
18. S. Gowtham, M. Deshpande, A. Costales, R. Pandey, *J. Phys. Chem. B*, 2005, ***109***, 14836.
19. N. Seeburrun, E. F. Archibong, P. Ramasami, *Chem. Phys. Lett*., 2008, ***467***, 23.

20. N. Seeburrun, H. H. Abdallah, E. F. Archibong, P. Ramasami, *Eur. Phys. J. D*, 2011, ***63***, 351.

21. N. Seeburrun, H. H. Abdallah, P. Ramasami, *J. Phys. Chem. A*, 2012, ***116***, 3215.

22. A. Köhn, B. Gaertner, H.-J. Himmel, *Chem. Eur. J.* 2005, ***11***, 5575.

23. B. Gaertner, A. Köhn, H.-J. Himmel, *Eur. J. Inorg. Chem.* 2006, ***11***, 1496.

24. N. Seeburrun, M. M. J. Soopramanien, H. H. Abdallah, E. F. Archibong, P. Ramasami, *J. Mater. Sci.* 2012, ***47***, 4332.

25. Gaussian 09, Revision **D.01**, M. J. Frisch, G. W. Trucks, H. B. Schlegel, G. E. Scuseria, M. A. Robb, J. R. Cheeseman, G. Scalmani, V. Barone, B. Mennucci, G. A. Petersson, H. Nakatsuji, M. Caricato, X. Li, H. P. Hratchian, A. F. Izmaylov, J. Bloino, G. Zheng, J. L. Sonnenberg, M. Hada, M. Ehara, K. Toyota, R. Fukuda, J. Hasegawa, M. Ishida, T. Nakajima, Y. Honda, O. Kitao, H. Nakai, T. Vreven, J. A. Montgomery, Jr., J. E. Peralta, F. Ogliaro, M. Bearpark, J. J. Heyd, E. Brothers, K. N. Kudin, V. N. Staroverov, R. Kobayashi, J. Normand, K. Raghavachari, A. Rendell, J. C. Burant, S. S. Iyengar, J. Tomasi, M. Cossi, N. Rega, J. M. Millam, M. Klene, J. E. Knox, J. B. Cross, V. Bakken, C. Adamo, J. Jaramillo, R. Gomperts, R. E. Stratmann, O. Yazyev, A. J. Austin, R. Cammi, C. Pomelli, J. W. Ochterski, R. L. Martin, K. Morokuma, V. G. Zakrzewski, G. A. Voth, P. Salvador, J. J. Dannenberg, S. Dapprich, A. D. Daniels, Ö. Farkas, J. B. Foresman, J. V. Ortiz, J. Cioslowski, and D. J. Fox, Gaussian, Inc., Wallingford CT, 2009.

26. S. Sriram, R. Chandiramouli, *Res. Chem. Intermed*., 2013, ***41***, 2095.

27. K. Kunkel, E. Milke, M. Binnewies, *Eur. J. Inorg. Chem*. 2015, ***1***, 124.

28. J. P. Perdew, *Phys. Rev. B*, 1986, ***33***, 8822.

29. J. P. Perdew, *Phys. Rev. B*, 1986, ***34***, 7406.

30. J. P. Perdew, Wang, Y. *Phys. Rev. B*, *1992*, ***45***, 13244.

31. J. P. Perdew, J. A. Chevary, S. H. Vosko, K. A. Jackson, M. R. Pederson, D. J. Singh, C. Fiolhais, *Phys. Rev. B*, 1992, ***46***, 6671.

32. C. Lee, W. Yang, R. G. Parr, *Phys. Rev. B*, 1988, ***37***, 785.

33. A. D. Becke, *J. Chem. Phys*., 1993, ***98***, 5648.

34. R. J. Bartlett, *Ann. Rev. Phys. Chem*., 1981, ***32***, 359.

35. W. J. Hehre, L. Radom, P. v. R. Schleyer, J. A. Pople, *Ab Initio Molecular Orbital Theory*; Wiley: New York, 1986.

36. K. Raghavachari, G.W. Trucks, J. A. Pople, M. Head-Gordon *Chem. Phys. Lett*., 1989, ***157***, 479.

37. A. E. Reed, R. B. Weinstock, F. Weinhold, *J. Chem. Phys*., 1985, ***83***, 735.

38. A. E. Reed, L. A. Curtiss, F. Weinhold, *Chem. Rev*., 1988, ***88***, 899.

39. G. Meloni, S. M. Sheehan, D. M. Neumark, *J. Chem. Phys.*, 2005, ***122***, 074317-1.

40. B. D. Fahlman, A. Daniels, G. E. Scusceria, A. R. Barron, *Dalton Trans*., 2001, 3239.

41. B. Eisenmann, A. *Z.* Hofmann, *Kristallgor*., 1991, ***197***, 145.

42. M. Julien-Pouzol, S. Jaulmes, M. Guittard, F. Alapini, *Acta Crystallogr*., 1979, ***35***, 2848.

43. F. Alapini, J. Flahaut, M. Guittard, S. Jaulmes, M. Julien-Pouzol, *J. Solid State Chem*., 1979, ***28***, 309.

44. S. A. Semiletov, V. A. Vlasov, *Kristallografiya*, 1963, ***8***, 877.

45. T. Chivers, J. S. Ritch, S. D. Robertson, J. Konu, H. M. Tuononen, *Acc. Chem. Res*., 2010, ***43***, 1053.

46. H. Hotop, W. C. Lineberger, *J. Phys. Chem. Ref. Data*, 1985, ***14***, 731.

47. Y. Zhao and D. G. Truhlar, *J. Chem. Phys*., 2006, ***124***, 224105-1-6.

48. M. M. Zhong, X. Y. Kuang, Z. H. Wang, P. Shao, L. P. Ding, *J. Mol. Model.*, 2013, ***19***, 263.

49. R. G. Pearson, *Chemical hardness: Applications from molecules to solids*. Wiley-VCH, Winheim, **1997**.

50. R. G. Parr and P. K. Chattaraj, *J. Am. Chem. Soc.*, 1991, ***113***, 1854.

Acknowledgments

N.S. acknowledges support from the Mauritius Tertiary Education Commission (TEC). The authors also acknowledge facilities from the University of Mauritius and the University of Namibia. The authors extend their appreciation to the Deanship of Scientific Research at King Saud University for the research group Project No. RGP VPP-207. The authors would like to thank the anonymous reviewers for useful comments to improve the manuscripts.

Supporting Information

Tables containing harmonic vibrational frequencies, ADEs, VDEs, VIPs (eV) and chemical hardness (η) of gallium telluride clusters.

Figures presenting the structural evolution of mono and digallium tellurides.

List of Tables

Table 1: Energy shifts (eV) of the first low-lying states with respect to ground states of the mono and digallium tellurides [Basis sets Ga: 6-311+G(2df) and Te: LANL2DZdp].

Methods	B3P86	B3PW91	B3LYP	MP2
GaTe	0.08	0.08	0.01	0.20
$GaTe^-$	2.19	2.14	2.20	2.21
$GaTe^+$	0.94	0.97	0.99	0.79
$GaTe_2$	0.18	0.18	0.18	0.01
$GaTe_2^-$	0.93	0.92	0.92	1.33
$GaTe_2^+$	0.35	0.35	0.34	0.35
$GaTe_3$	0.12	0.12	0.19	0.60
$GaTe_3^-$	0.80	0.81	0.71	1.45
$GaTe_3^+$	0.14	0.15	0.05	0.83
$GaTe_4$	0.09	0.07	0.17	–0.23
$GaTe_4^-$	0.21	0.19	0.28	–0.02
$GaTe_4^+$	0.20	0.21	0.11	0.63
Ga_2Te	0.14	0.14	0.13	0.19
Ga_2Te^-	0.49	0.48	0.42	0.45
Ga_2Te^+	0.12	0.13	0.12	0.28
Ga_2Te_2	0.57	0.57	0.49	0.33
$Ga_2Te_2^-$	0.62	0.61	0.54	0.65
$Ga_2Te_2^+$	0.39	0.39	0.38	0.43
$Ga_2Te_3^+$	0.19	0.20	0.17	0.67
Ga_2Te_4	0.17	0.18	0.28	0.44
$Ga_2Te_4^-$	0.23	0.23	0.22	0.60
$Ga_2Te_4^+$	0.19	0.20	0.12	0.77

Table 2: Adiabatic electron affinities (AEAs) of the gallium telluride clusters using different levels of theory [Basis sets Ga: 6-311+G(2df) and Te: LANL2DZdp].

Cluster	B3P86	B3PW91	B3LYP	MP2	CCSD(T)//B3LYP
GaTe	3.20	2.65	2.67	2.48	2.46 (2.57)[a], **2.46**[b]
$GaTe_2$	3.83	3.29	3.23	3.55	3.46 (3.38)
$GaTe_3$	3.94	3.40	3.31	3.20	3.23 (3.50)
$GaTe_4$	3.81	3.27	3.24	3.23	3.10 (3.30)
Ga_2Te	1.92	1.39	1.25	1.32	1.33 (1.37)
Ga_2Te_2	2.95	2.40	2.35	2.49	2.46 (2.34)
Ga_2Te_3	3.71	3.18	3.02	2.77	2.77 (3.10)
Ga_2Te_4	4.07	3.51	3.50	3.14	3.01 (3.41)

[a] AEA values in parenthesis were obtained using single point CCSD(T) with def2-TZVP basis set

[b] AEA value in bold was obtained at the CCSD(T) level of theory

Table 3: Adiabatic ionization potentials (AIPs) of the gallium telluride clusters using different levels of theory [Basis sets Ga: 6-311+G(2df) and Te: LANL2DZdp].

Cluster	B3P86	B3PW91	B3LYP	MP2	CCSD(T)//B3LYP
GaTe	8.82	8.25	8.17	8.08	7.85 (8.20)[a], **8.01**[b]
$GaTe_2$	8.36	7.80	7.65	7.73	7.84 (7.75)
$GaTe_3$	7.84	7.29	7.36	7.08	6.85 (7.13)
$GaTe_4$	7.64	7.08	7.14	6.45	6.52 (6.92)
Ga_2Te	8.21	7.65	7.62	7.54	7.55 (7.63)
Ga_2Te_2	8.22	7.65	7.51	7.27	7.13 (7.64)
Ga_2Te_3	7.66	7.10	7.22	6.92	6.86 (7.03)
Ga_2Te_4	7.54	7.00	7.10	6.80	6.93 (6.95)

[a] AIP values in parenthesis were obtained using single point CCSD(T) with def2-TZVP basis set

[b] AIP value in bold was obtained at the CCSD(T) level of theory

Table 4: Dissociation energies (D_e, kJ/mol) of gallium tellurides through different channels [Basis sets Ga: 6-311+G(2df) and Te: LANL2DZdp].

Channels					**B3P86**	**B3PW91**	**B3LYP**	**MP2**	**CCSD(T)//B3LYP**
GaTe	→	Ga	+	Te	282.3	272.6	259.6	266.2	260.5
$GaTe_2$	→	Ga	+	Te_2	266.5	258.4	243.8	275.7	265.9
$GaTe_2$	→	GaTe	+	Te	274.7	266.2	252.9	234.9	224.1
$GaTe_2$	→	Ga	+	2Te	557.0	538.8	512.5	501.0	484.7
$GaTe_3$	→	GaTe	+	Te_2	169.5	163.4	144.2	217.3	192.1
$GaTe_3$	→	$GaTe_2$	+	Te	185.4	177.6	159.9	207.7	186.7
$GaTe_3$	→	GaTe	+	2Te	460.1	443.8	412.8	442.6	410.8
$GaTe_4$	→	$GaTe_2$	+	Te_2	139.2	131.9	105.9	196.9	171.4
$GaTe_4$	→	GaTe	+	Te_3	232.4	225.8	207.7	294.2	264.8
$GaTe_4$	→	$GaTe_3$	+	Te	244.3	234.6	214.6	214.2	203.4
$GaTe_4$	→	Ga	+	$2Te_2$	405.7	390.3	349.7	472.6	437.3
Ga_2Te	→	GaTe	+	Ga	293.1	285.4	282.6	284.7	276.3
Ga_2Te	→	2Ga	+	Te	575.4	558.0	542.2	550.9	536.8
Ga_2Te_2	→	2GaTe			265.1	258.8	242.2	236.6	235.9
Ga_2Te_2	→	Ga_2Te	+	Te	254.4	246.0	219.1	238.1	220.2
Ga_2Te_2	→	$GaTe_2$	+	Ga	272.8	262.2	248.9	288.0	272.3
Ga_2Te_3	→	Ga_2Te	+	Te_2	172.6	166.3	136.0	278.6	253.6
Ga_2Te_3	→	GaTe	+	$GaTe_2$	199.1	193.3	174.8	287.6	263.9
Ga_2Te_3	→	Ga_2Te_2	+	Te	208.7	200.7	185.5	265.8	252.2
Ga_2Te_3	→	Ga_2Te	+	2Te	463.1	446.7	404.6	503.9	472.3
Ga_2Te_4	→	Ga_2Te_2	+	Te_2	165.5	161.2	131.1	279.1	272.4
Ga_2Te_4	→	$2GaTe_2$			171.2	168.1	136.1	291.3	278.8
Ga_2Te_4	→	$GaTe_3$	+	GaTe	261.1	256.6	229.1	318.4	316.2
Ga_2Te_4	→	Ga_2Te_3	+	Te	247.3	241.0	214.3	238.6	239.0
Ga_2Te_4	→	Ga_2Te_2	+	2Te	456.0	441.6	399.7	504.3	491.1

List of Figures

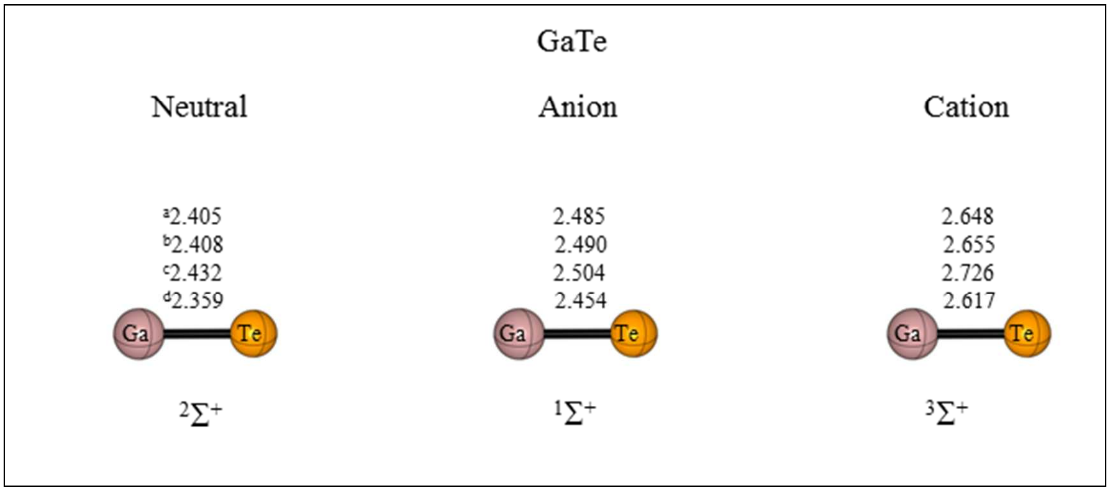

Fig. 1: Geometrical features of diatomic GaTe with the electronic states [Basis sets Ga: 6-311+G(2df) and Te: LANL2DZdp].

[a]B3P86, [b]B3PW91, [c]B3LYP and [d]MP2

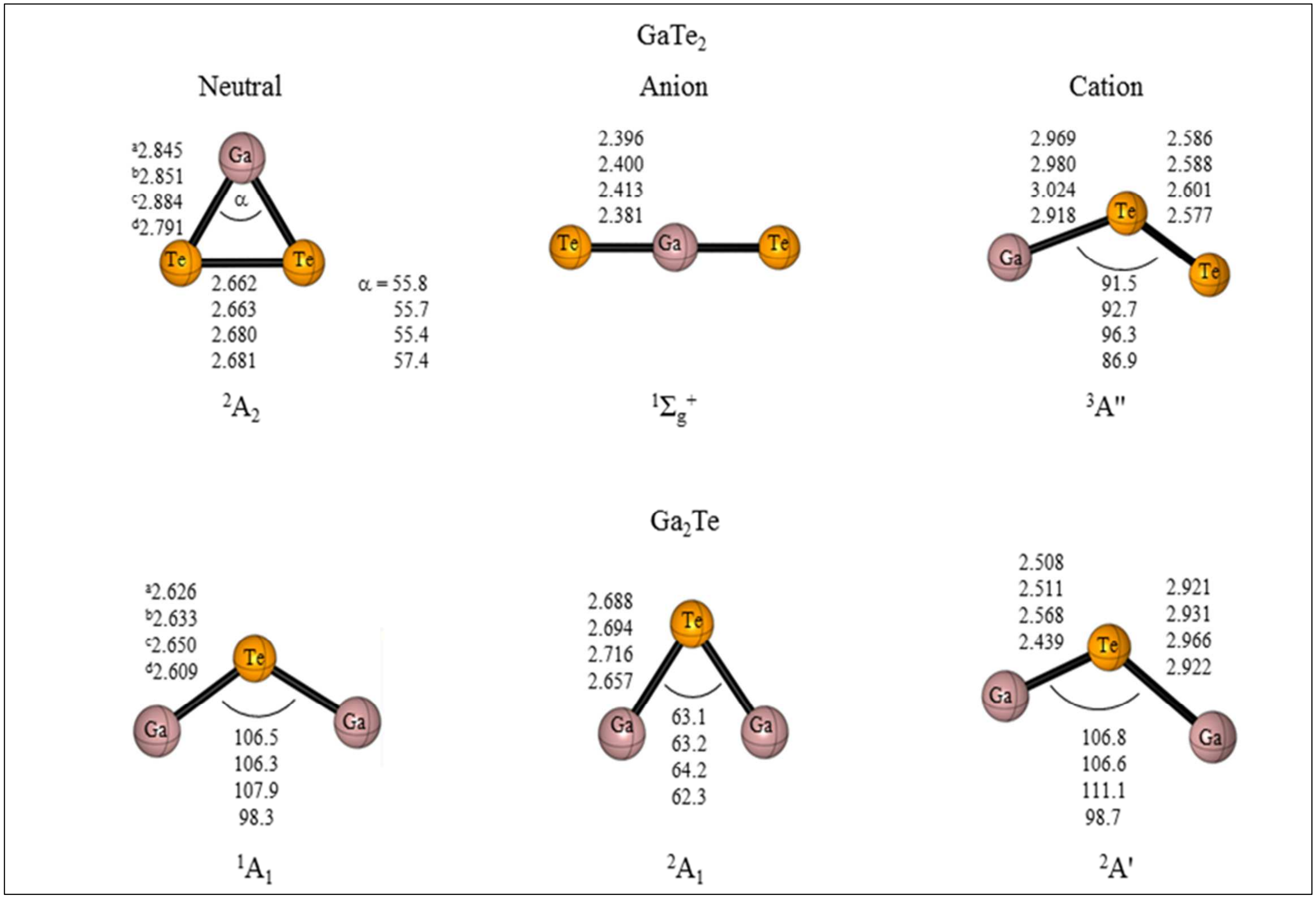

Fig. 2: Geometrical features of $GaTe_2$ and Ga_2Te with the electronic states [Basis sets Ga: 6-311+G(2df) and Te: LANL2DZdp].

[a]B3P86, [b]B3PW91, [c]B3LYP and [d]MP2

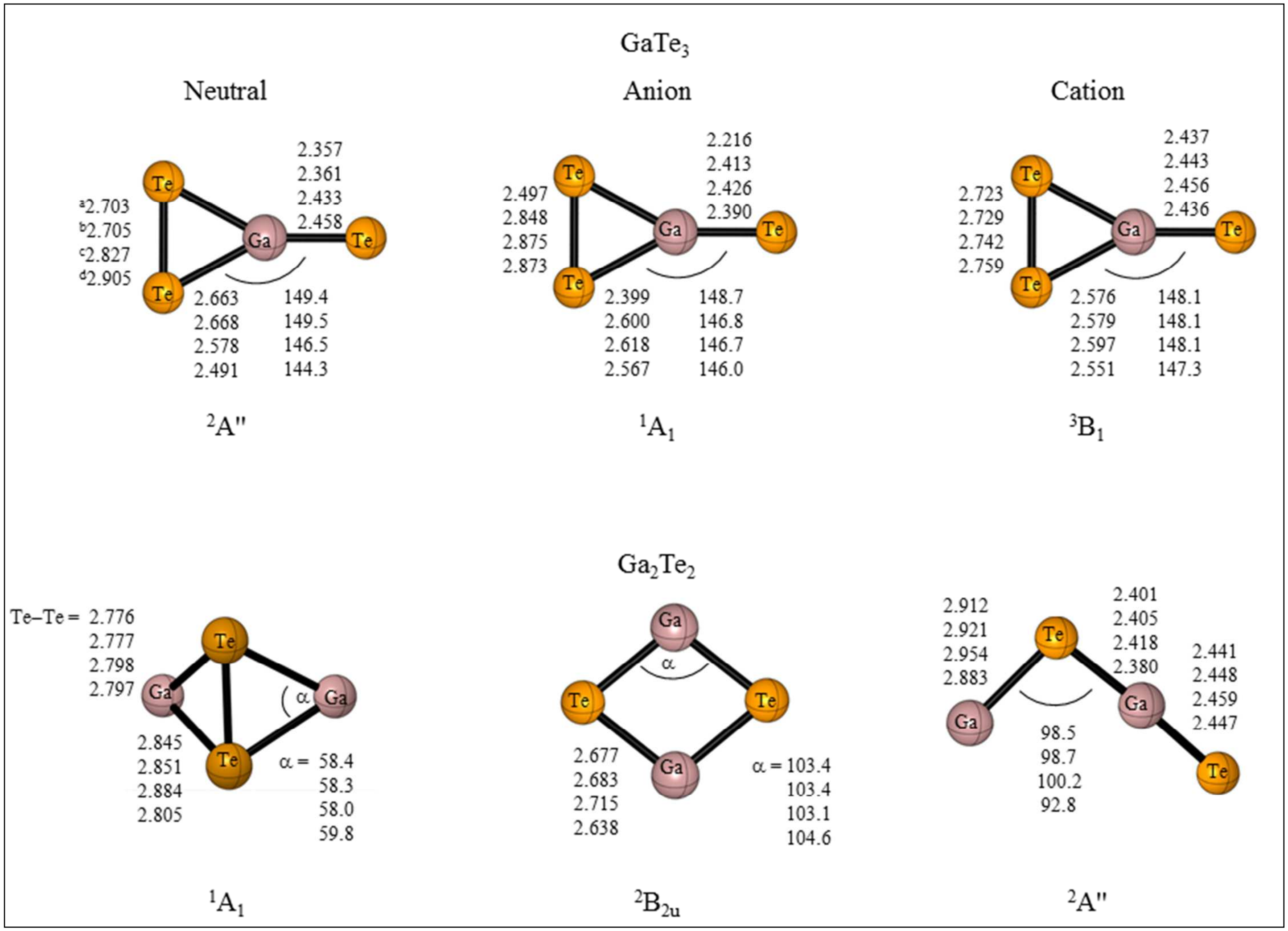

Fig. 3: Geometrical features of $GaTe_3$ and Ga_2Te_2 with the electronic states [Basis sets Ga: 6-311+G(2df) and Te: LANL2DZdp].

[a]B3P86, [b]B3PW91, [c]B3LYP and [d]MP2

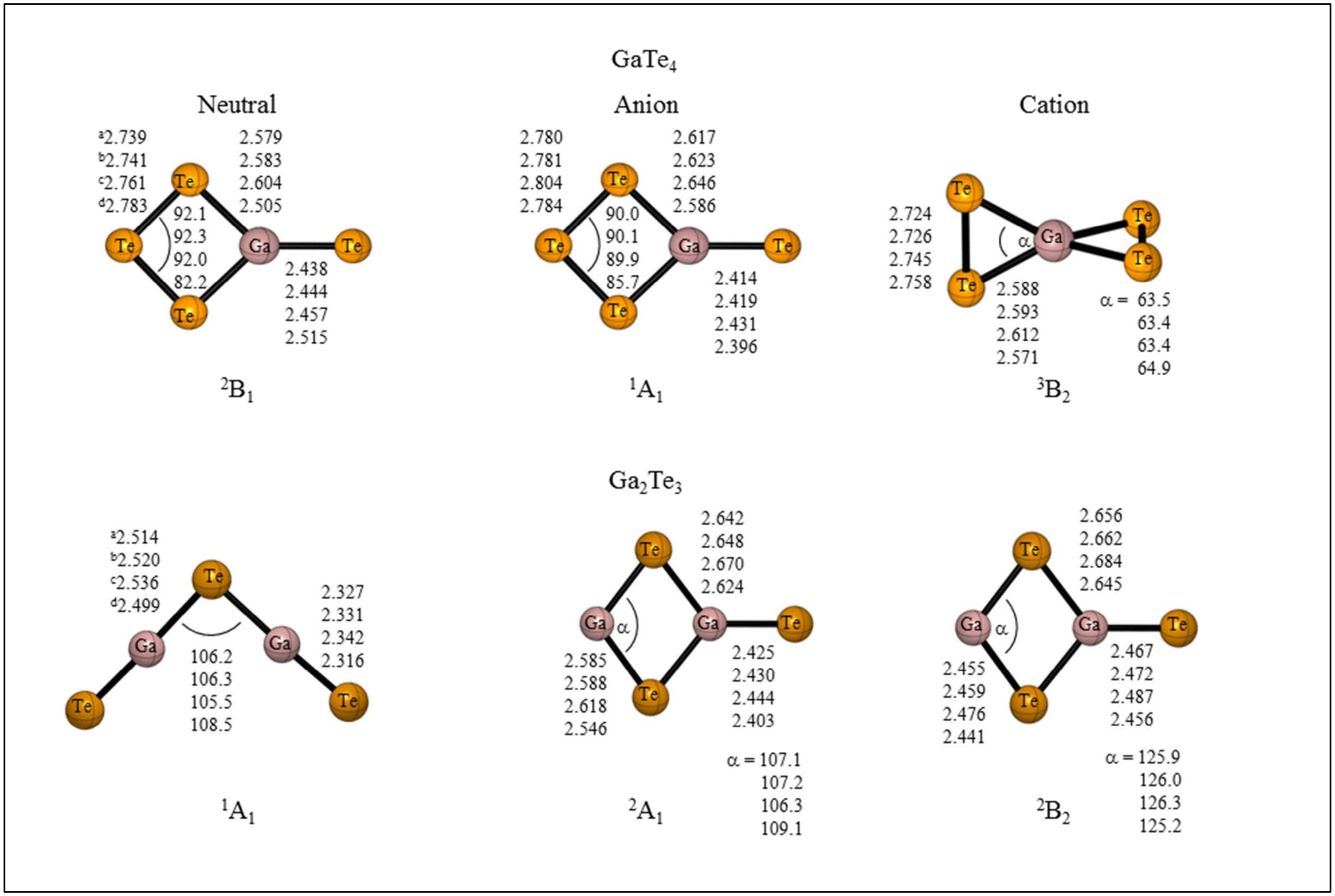

Fig. 4: Geometrical features of $GaTe_4$ and Ga_2Te_3 with the electronic states [Basis sets Ga: 6-311+G(2df) and Te: LANL2DZdp].

^{a}B3P86, ^{b}B3PW91, ^{c}B3LYP and ^{d}MP2

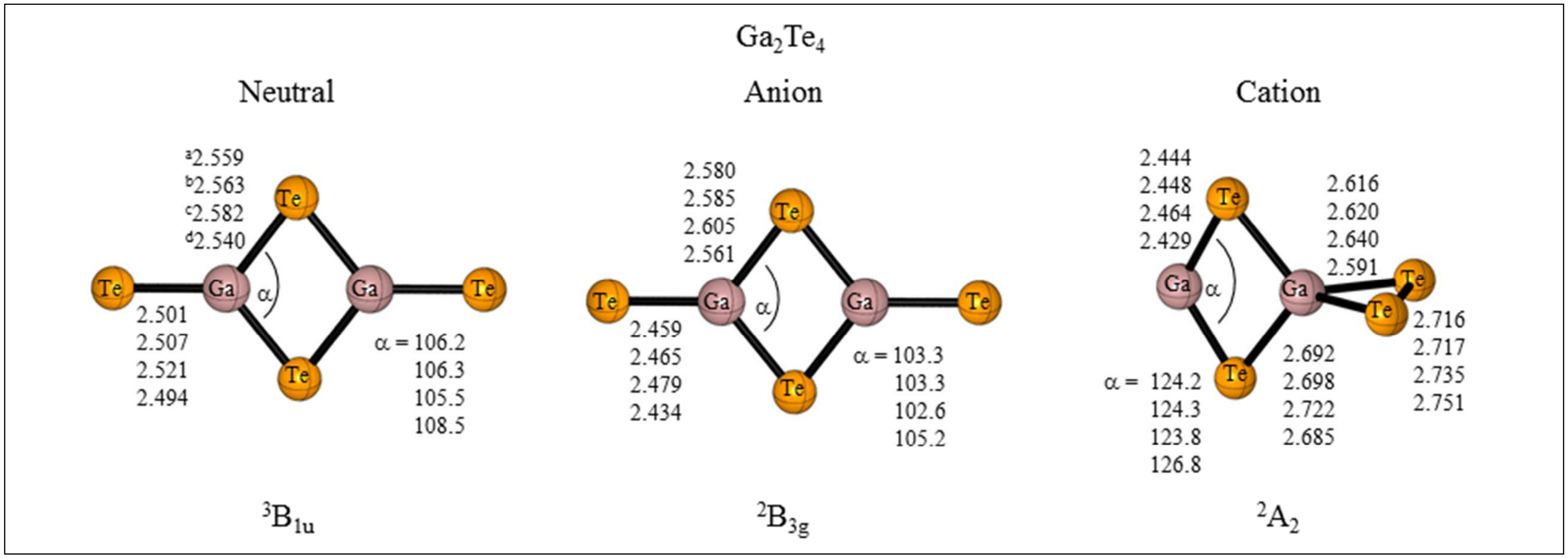

Fig. 5: Geometrical features of Ga_2Te_4 with the electronic states [Basis sets Ga: 6-311+G(2df) and Te: LANL2DZdp].

[a]B3P86, [b]B3PW91, [c]B3LYP and [d]MP2

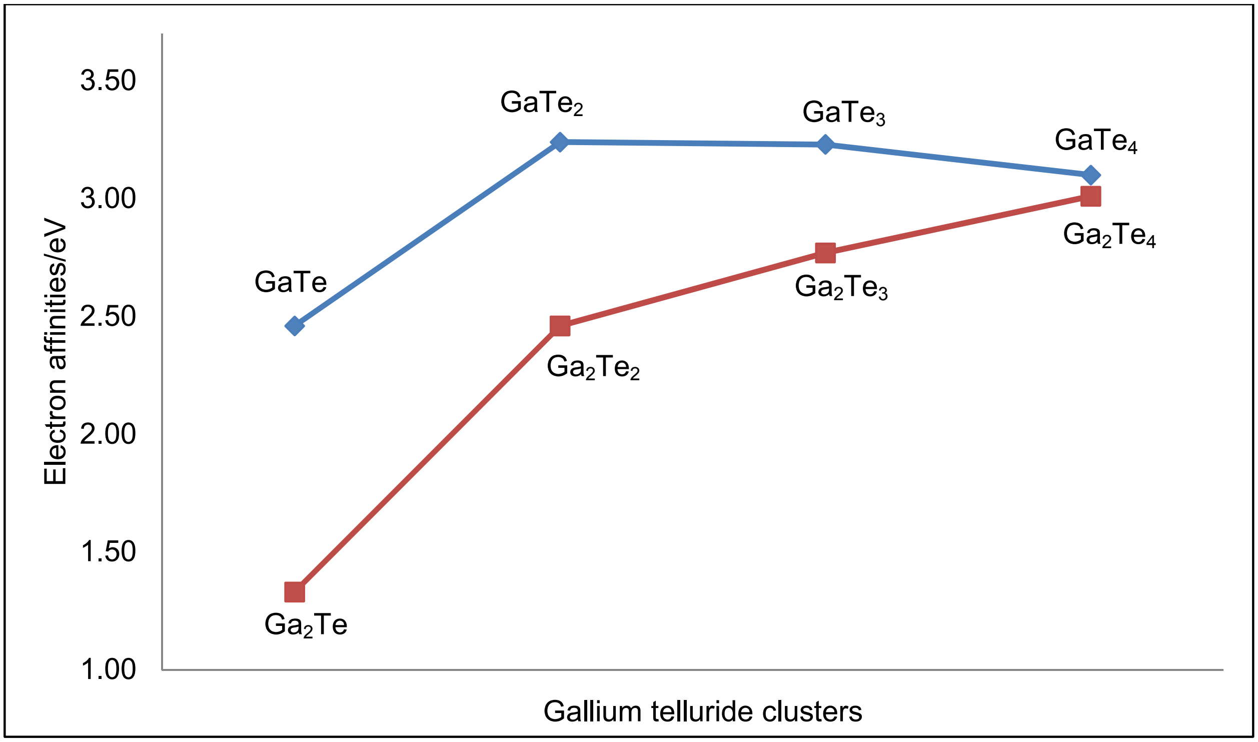

Fig. 6: Electron affinities of the gallium telluride clusters at the CCSD(T)//B3LYP level [Basis sets Ga: 6-311+G(2df) and Te: LANL2DZdp].

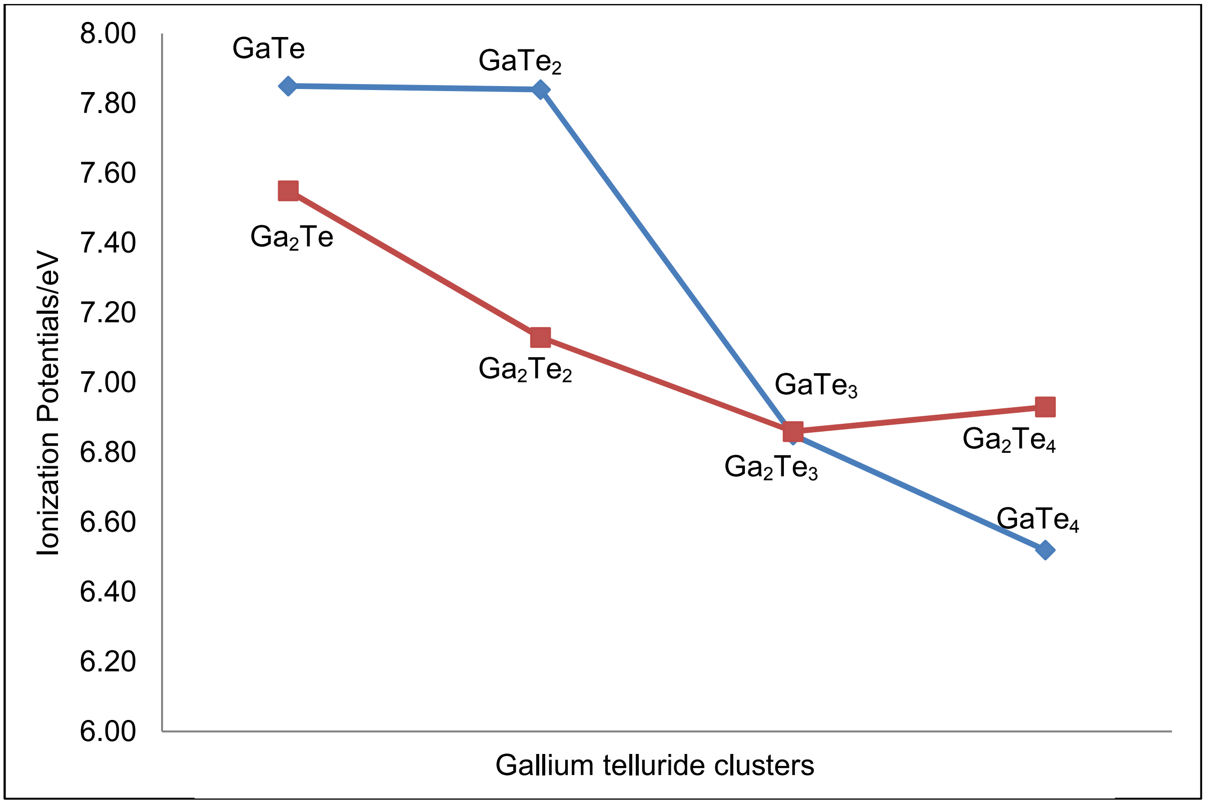

Fig. 7: Ionization potentials of the gallium telluride clusters at the CCSD(T)//B3LYP level [Basis sets Ga: 6-311+G(2df) and Te: LANL2DZdp].